agriculture

MDPI

Article

Multi-Tooth Cutting Method and Bionic Cutter Design for Broccoli Xylem (*Brassica oleracea* L. var. Italica Plenck)

Yunlong Cao, Yao Yu, Zhong Tang *, Yunfei Zhao, Xinyang Gu, Sifan Liu and Shuren Chen

School of Agricultural Engineering, Jiangsu University, Zhenjiang 212013, China; 2212216060@stmail.ujs.edu.cn (Y.C.); 3200306031@stmail.ujs.edu.cn (Y.Y.); 2212016038@stmail.ujs.edu.cn (Y.Z.); 2212116078@stmail.ujs.edu.cn (X.G.); 2222116076@stmail.ujs.edu.cn (S.L.); srchen@ujs.edu.cn (S.C.)
* Correspondence: zht@ujs.edu.cn

Abstract: During the harvesting of cut-stem vegetables, the structural parameters of cutters have an important influence on the harvesting effect. Structural parameters of stalks directly affect the cutting effect of the cutter. The thickness of the stalk xylem has a strong influence on the cutting stability and cutting surface effect of the cutter. In this paper, the effect of the broccoli stalk xylem on conventional toothless cutters was investigated using broccoli stalks as the cutting object. It was found that a thicker xylem leads to shear force fluctuations, which in turn affects the smooth operation of the cutting device. Taking locust mouthparts as the research object, a bionic multi-tooth cutting method is proposed in this paper to obtain the contour curve based on the locust upper jaw cutting tooth lobe. By establishing the regression equation, the contour curve of the cutting teeth is fitted accurately. The cutter edge is designed with the locust's maxillary incisive lobe as the bionic object. ANSYS software was used to simulate the cutting of a double disc cutter and broccoli stalk. The effect of each factor was analyzed by response-surface regression to determine the optimal cutter speed, machine forward speed, cutting inclination, blade overlap, and optimal cutting position. The cutting test is verified via broccoli stalks and a cutting test bench to further determine the cutting device operating parameters. The optimal operating parameters of the cutting device were 0.239 m/s forward speed, 30.974-degree cutting edge angle, 10.066 mm blade overlap, and 467.511 rpm.

Keywords: broccoli stem; cutting device; bionic method; locust mandibular incisor

Citation: Cao, Y.; Yu, Y.; Tang, Z.; Zhao, Y.; Gu, X.; Liu, S.; Chen, S. Multi-Tooth Cutting Method and Bionic Cutter Design for Broccoli Xylem (*Brassica oleracea* L. var. Italica Plenck). *Agriculture* **2023**, *13*, 1267. https://doi.org/10.3390/agriculture13061267

Academic Editor: Mustafa Ucgul

Received: 31 May 2023
Revised: 14 June 2023
Accepted: 16 June 2023
Published: 19 June 2023

1. Introduction

Broccoli (*Brassica oleracea* L. var. Italica Plenck) is a healthy vegetable known for its rich content of bioactive components such as vitamins, antioxidants, and anticancer precursors [1–3]. Broccoli is widely grown in China with a planted area of more than 76,000 hm^2 which is increasing year by year [4]. Broccoli stalks account for 35% of the broccoli harvest residue and the accompanying unused waste generated needs to be recycled to contribute to the sustainability of the system [5]. Plant stalks are composite materials with cellulose, hemicellulose, and lignin as the main chemical components [6]. Studies on the material and mechanical properties of broccoli stalks have been reported [7]. The cutting of crop stems is a key process for the automation and intelligence of harvesting. Therefore, the mechanical properties of the harvesting process have attracted a lot of attention in recent decades. Images of broccoli from field cutting to harvested products are shown in Figure 1.

Cutting is an essential process for agricultural products, such as broccoli, where injury pressure is inevitably generated [8]. The type of cutting and storage affects the bacterial diversity of freshly cut broccoli, which is important for the food industry to provide control of microbial contamination and prolong food shelf life [9,10]. Moisture content and cutting surface area have significant effects on the mechanical cutting performance of sugarcane stalks, and peak force, cutting energy, ultimate stress, and specific energy have been determined experimentally [11]. An empirical equation and mechanical model for

the unit cutting force of sugarcane straw have been established. The significant effects of cutting speed, cutting position, and forward speed on stubble damage have been analyzed by high-speed photography [12]. Xu et al. further designed a cabbage-harvesting knife with a convex curve based on shear characteristic tests [13]. A mechanical model for cutting cabbage roots via a single-point clamping method was developed to obtain the optimal cutting combination based on single- and multi-factor cutting tests to reduce damage [14]. To evaluate the mechanical cutting characteristics of corn stalks, their blunt-edged cutting elements were replaced with cutting elements having a single beveled pointed blade of 30 degrees [15].

(**a**) Broccoli stalk (**b**) Broccoli after harvest (**c**) Broccoli cutting root

Figure 1. The harvest of broccoli.

The application of animal physiology and morphology in the design of agricultural machinery has received much attention in recent years. Bionics has been applied to the design of tool components such as openers, plows, and stubble rotators to reduce resistance and reduce energy consumption [16]. Bionics has provided researchers with new research ideas and effective research methods to solve various problems, including energy saving and improving the quality of tools. Serrated teeth are a prominent feature of many fish teeth, and rodents' teeth are constantly sharpened to ensure their sharpness and efficacy [17]. A bionic blade was designed for a comparative test of corn-stover cutting performance by extracting the cutting tooth profile curve of the upper jaw using bionic principles. The bionic blade had a superior performance as shown by its high cutting ability and good cutting quality. A mechanical model of the mechanism cutting carrot stalk and leaves was established by fitting and optimizing the original morphology with the tibial curve of the forelimb of the mantis; the conditions for efficient cutting were verified and determined by this model, and the influencing factors of the feeding speed of the carrot and the operating performance of the disc cutting device were determined [18,19].

The simulation model established by ANSYS/LS-DYNA 19.0 software was used to simulate the soil-cutting process of bionic cutting teeth, and the results showed that cutting teeth with a bionic structure can effectively reduce the average cutting resistance, cutting stress, soil energy, and maximum cutting resistance to obtain a soil cutting effect [20]. A high-performance coupled bionic stubble-cutting device based on a locust mouth tooth structure was used to solve technical problems such as the low efficiency of corn stubble crushing, high cutting torque, and high power consumption [21]. Therefore, based on the unique morphological structure and geometric features of the organism, the application

of bionic components in the optimal design of agricultural machinery components can achieve better working results [22]. A bionic cutting knife inspired by the special geometry of cricket teeth was designed to reduce the force and energy required to cut tea tree stalks, and the optimal operating parameters of the cutting device were determined [23,24]. It was also investigated whether the multi-coupled motion-structure-material bionic design could further improve the cutting performance [25]. Bionics has been heavily applied to the engineering field to provide directions for solving scientific and technological challenges by studying the structural properties of living things.

The use of the bionic principle can obtain a better technical solution, reasonable mechanical structure, and lower energy consumption. Based on the bionic principle, this paper designs a broccoli stalk cutting device with double disc knives rotating at equal speed for cutting based on morphological simulation combined with a motion behavior bionic. This is achieved according to the morphological characteristics of locust mouthparts' structure and the motion form of cutting plant fibers.

2. Materials and Methods

2.1. Mechanical Test of Broccoli Xylem

The mechanical testing of the broccoli xylem is performed with the TA.XTPLUS Texturizer (Stable Micro System, London, UK), which is capable of performing many forms of mechanical tests by changing the indenter of various models. The test items include stem shear.

When broccoli is harvested, the stalk-cutting position is 50–100 mm below the flower bulb. This section of the broccoli stalk was selected, and five measurement points were selected on the broccoli stalk in the order of top to bottom, with a 10 mm interval between each measurement point. As shown in Figure 2, a physical property tester was used to perform the broccoli stalk shear test. The blade was moved downward with a displacement of 15 mm, a speed of 1 mm/s, and a data sampling interval of 0.005 s.

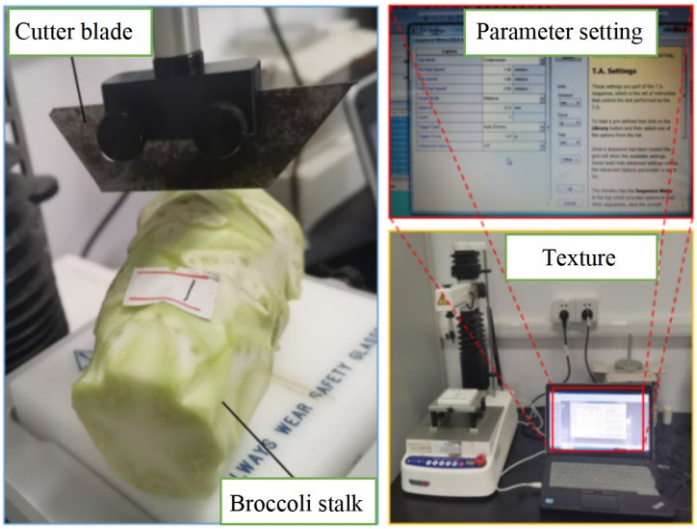

Figure 2. Shear mechanical properties test of the xylem of broccoli.

2.2. Exploration of Cutting Theory and Creation of Cutting Models

To further investigate the cutting theory of stalks with woody parts, the stalk-cutting model was first established and simulated by Ansys. The simplified stalk-cutting model was created in Solid Works, a 3D modeling software, and the corresponding solid model included a broccoli stalk and a disc cutter. The method is as follows.

Double-click on Model to enter Mechanical [ANSYS Mechanical Enterprise PrepPost]. Click on Model to expand the submenu, and assign material properties to each entity in Geometry, with the stiffness of the cutter as a rigid body and the stalk entity as a flexible

body. To facilitate the addition of loads and constraints, establish a local coordinate system in Coordinate Systems with the two disc cutters as the center. Click on Contacts under Connections to add contact properties to the model, the contact type of the epidermis, xylem, and pith of the broccoli stalk is Bonded, the contact between the disc cutter and the stalk is Face-to-Face contact, the contact type is Frictional, and the friction coefficient is 0.3. Select mesh partition to generate mesh. Then, the mesh size of the stalk entity is changed to 2 mm for mesh refinement. The initial angular velocity of the two disc knife entities is set in Initial Conditions under Workbench LS-DYNA by the created local coordinate system, the end time in Analysis Settings is set according to the solution, and the rest of the parameters are kept as default.

To simulate the broccoli-harvesting condition, fixed support constraints are added to the upper and lower sections of the stalk entity, and remote displacements are added to the two disc knives, such that the disc knives produce planar feed displacements and relative rotation constraints, as shown in Figure 3. Click Solution to solve, and the stalk-cutting fracture model is shown in Figure 4 after the solution is completed to evaluate the overall deformation, equivalent force, and contact stress of the model.

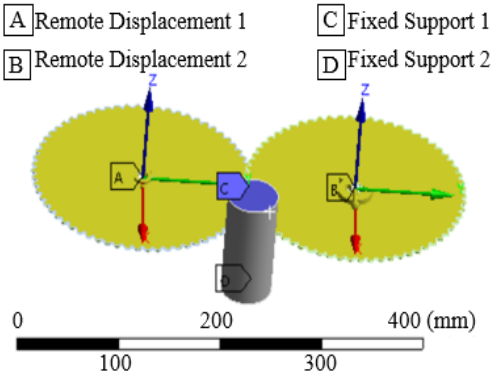

Figure 3. Broccoli stalk-cutting model.

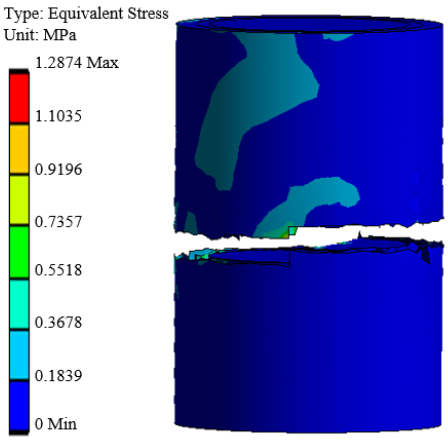

Figure 4. Equivalent stress of stem cutting.

2.3. Cutting Simulation Design

2.3.1. Single Factor Cutting Simulation Design

There are many factors influencing the broccoli stalk-cutting process. To study the influence of each factor on the cutting effect of broccoli stalks, a single-factor simulation was conducted by controlling variables. The disc cutter feed speed, cutting edge angle, overlap of two discs, and disc cutter speed were selected as variables, and five level values were selected for each variable. As shown in Table 1, the feed speed ranged from 0.01 to

0.41 m/s, the cutting edge angle from 5 to 45 degrees, the overlap amount from 1 to 21 mm, and the disc knife speed from 200 to 1000 rpm.

Table 1. Simulation factors and levels of cutting broccoli stems.

Level	Factor			
	Feed Speed/m/s	Cutting Edge Angle/Degrees	Overlap Amount/mm	Rotational Speed/rpm
1	0.01	5	1	200
2	0.11	15	6	400
3	0.21	25	11	600
4	0.31	35	16	800
5	0.41	45	21	1000

2.3.2. Multi-Factor Cutting Simulation Design

The broccoli stalk-cutting process is subject to the simultaneous action of several factors. To investigate the effect of multi-factor interaction on the cutting effect of broccoli stalks, a multi-factor simulation orthogonal test was designed based on the single-factor simulation results. The factor levels and responses are shown in Table 2, with cutter feed speeds of 0.21, 0.26, and 0.31 m/s, cutter cutting edge angles of 5, 15, and 25 degrees, cutter overlap of 1, 6, and 11 mm, and cutter speeds of 600, 800, and 1000 rpm.

Table 2. Simulation factors, level, and responses of cutting broccoli stems.

Factor	Units	Level			Response	Units
A: Feed speed	m/s	0.21	0.26	0.31	Y1: stem maximum equivalent stress	MPa
B: Cutting edge angle	degrees	5	15	25	Y2: advance speed fluctuation peak value	mm/s
C: Overlap amount	mm	1	6	11	Y3: Maximum contact force	N
D: Rotational speed	rpm	600	800	1000		

2.4. Bionic Object Morphological Model Theory

Locusts, which belong to the order Orthoptera, are commonly known as "grasshoppers", and their serrated incisive teeth have the advantageous ability to cut plant fibers. In this paper, the East Asian locust, which has a wide distribution in China, has a very diverse diet, mainly feeding on plants of the grass and sedge families, such as reeds, barnyard grass, corn, sorghum, rice, and sugarcane [26]. Locusts rely on chewing mouthparts to feed, and the movement of their mouthparts is reciprocating.

The live locusts used in this paper were taken from the northern region of Anhui Province, China, and were 4–6 cm in length. After their natural death, the upper jaw part of the locust was intercepted and dried in a ventilated place. The locusts were placed under a digital microscope (VHX-900F, Osaka, Japan) to observe the upper jaw of the locust mouthparts, as shown in Figure 5, and the focus knob was adjusted to obtain pictures after the images were clear.

The structure of the locust's upper jaw was observed using 50× magnification. The anterior part of the upper jaw is a cutting tooth area with sharp teeth for cutting food, and the posterior part is a rough grinding tooth for grinding food. The structure of the cutting lobe of the East Asian locust mainly consists of three large teeth and two small teeth arranged at intervals, with the top of each sharp tooth being rounded and curved, and the top of the middle tooth being higher than the other teeth, with an overall staggered distribution.

To extract the contour of the incisive lobe, the microscopic image of the locust's upper jaw was captured and enlarged, and the detailed image of the incisive lobe was imported into MATLAB R2021b software for processing. Since the obtained contour structure of the incisor lobe is a physical image with certain chromatic aberration and background vignetting, the curved contour cannot be extracted with high accuracy, so further processing

of the contour curve is required. Using the image-processing module in MATLAB software, the contour image is converted into a parametric mathematical model through the function command in the software according to the theory of mathematical morphology, and the exact function coordinates are finally obtained.

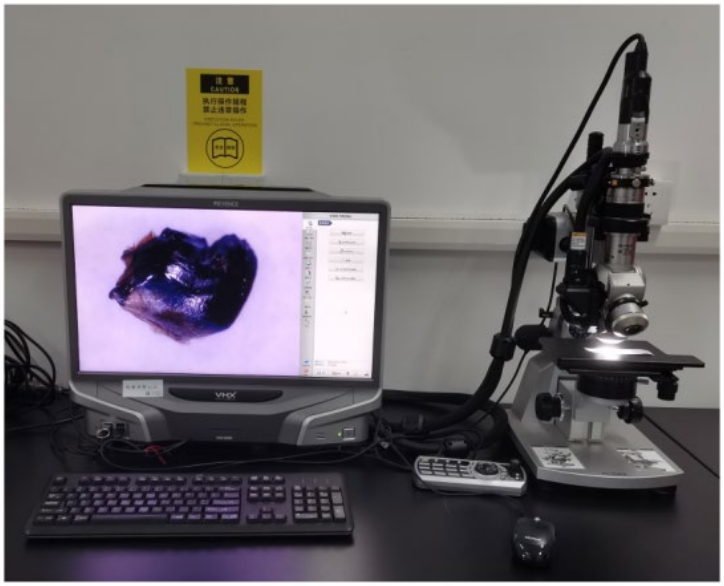

Figure 5. Micrograph of a locust's maxilla.

The specific method flow of locust epiglottis image processing is shown in Figure 6. To avoid the stray colors in the original image from interfering with the results, the colored original image is first converted into a grayscale image using the rgb2gray command; the redundant structural elements in the original image are also converted together, and the defocused areas can lead to computational errors. To make the transition between the image pixels more natural, the improved command is used to corrupt the edges of the grayscale image to obtain corrupted images. Then, an immediate command is used to inflate the contour and fill the corrupted area with natural color to ensure that both sides of the contour curve are clear and complete. Then, the image is binary converted using the im2bw command to make the image uniform in terms of numerical data, removing unnecessary data information and retaining only the pixel position and sampling information. Finally, boundary detection is performed and contour lines are extracted with the help of the edge function, edge extraction is performed using the canny operator, and the obtained contour coordinate values are saved in a two-dimensional coordinate system format.

The locust tangent lobe boundary contour curve is obtained according to the processing result of MATLAB software, as shown in Figure 7. The curve is placed in a dot matrix of 342 $\times$ 187 pixels. The locust tangent lobe boundary curve has three obvious wave peaks, and in the function fitting, if the overall curve fitting is used, no matter what fitting equation is used, the whole waveform characteristics cannot be perfectly restored. To ensure fitting accuracy, the boundary contour is divided into three independent curves with a single wave peak, which are named Curves 1–3.

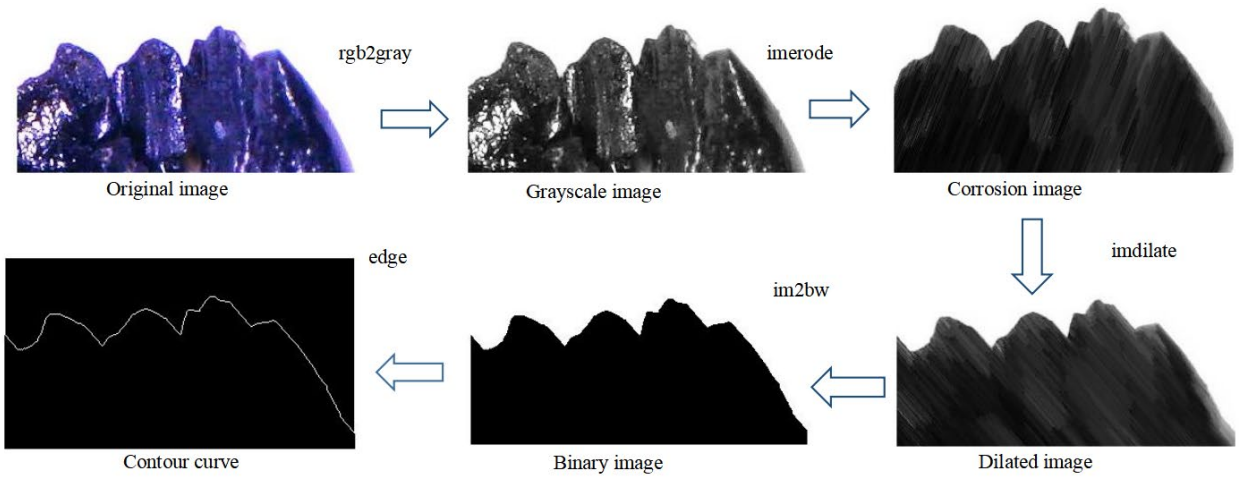

Figure 6. Processing of the image of a grasshopper's incisor lobe.

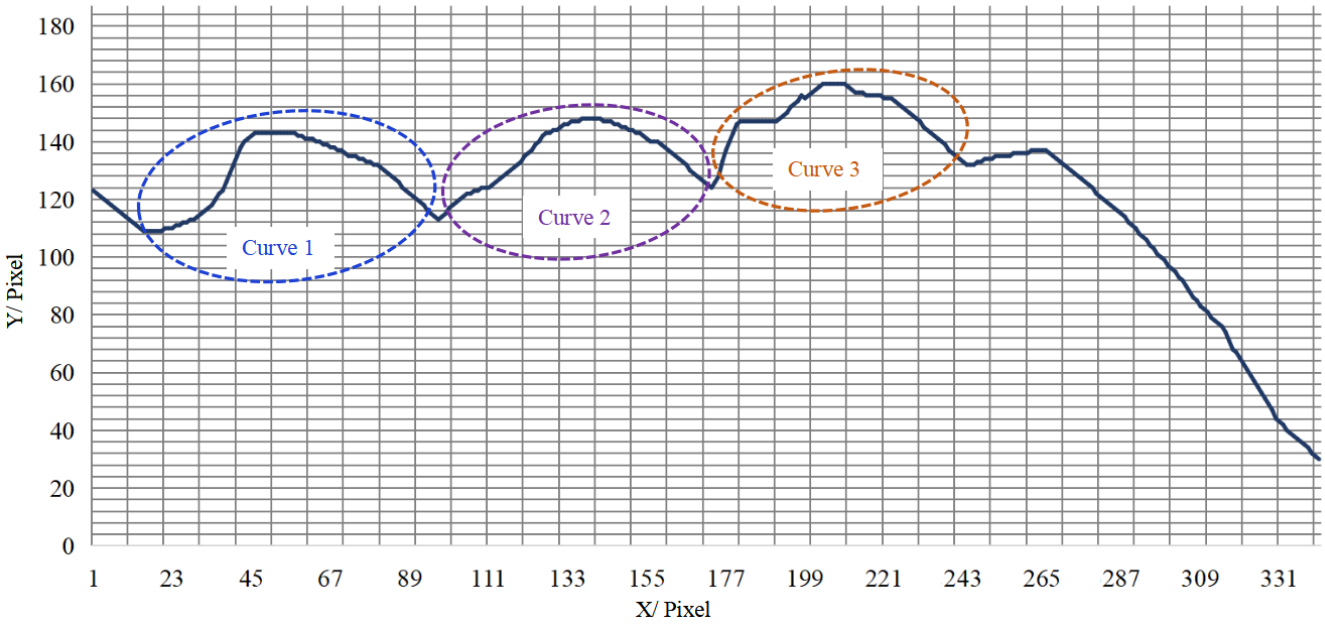

Figure 7. Contour curve of a locust's incisor lobe.

2.5. Bench Comparison Test

To verify the accuracy of the simulation conclusions, broccoli stalk-cutting tests were carried out to further investigate the advantages of the bionic cutter. One disc conventional cutter and three bionic cutters were trialed for this purpose to further compare and verify the different cutter operations and cutting effects by the test method, as shown in Figure 8 below.

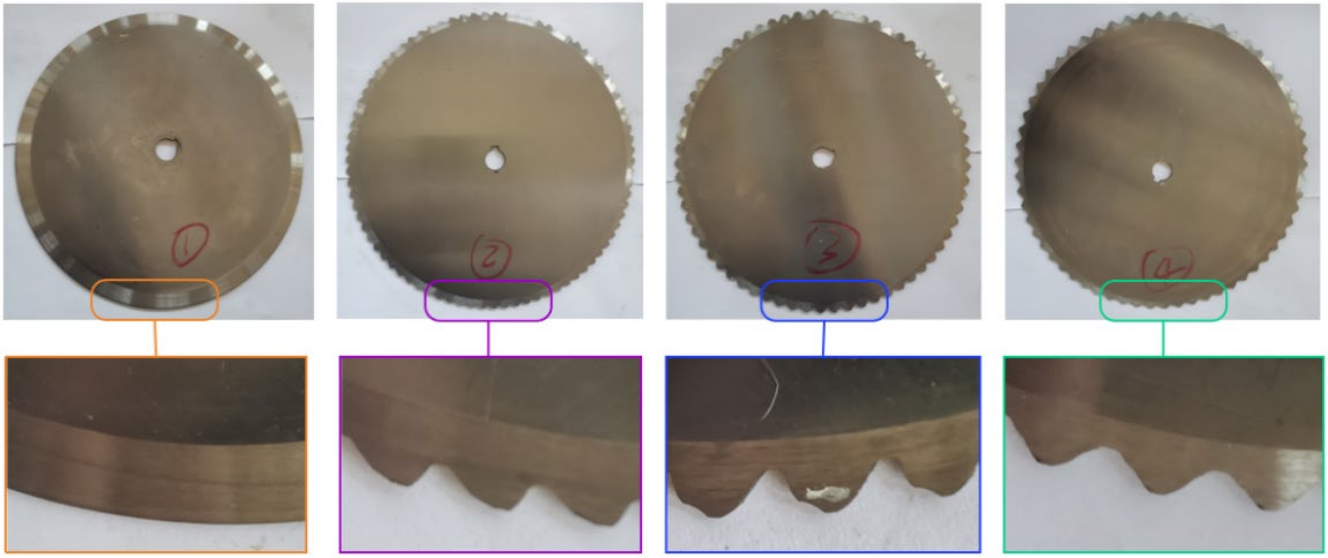

Figure 8. Sample of the circular cutters. (**a**) Conventional cutter. (**b**) Bionic Cutter I. (**c**) Bionic Cutter II. (**d**) Bionic Cutter III.

In the broccoli stalk-cutting test, the stalk is fixed to the holder by clamping, and the motor mounting position is adjusted such that the overlap of the two disc cutters reaches the specified value. After turning on the power, the knobs of the two motor governors are turned to adjust the cutter speed. Due to voltage fluctuations and other reasons, the cutter speed may have errors with the test conditions; the contact tachometer can be used to measure the cutter speed and adjust the motor governors again to ensure the cutter speed matches the test conditions. The retracting speed of the electric culm pusher is adjusted through the knob of the culm pusher governor. When the operating conditions of the test bench match with the test conditions, the culm must be pushed through the culm pusher controller to push the stalk to the cutter. Before the stalk touches the cutter, the contact head of the contact tachometer must be pressed smoothly onto the shaft end of the motor. After the stalk has been cut, the tachometer measurement key must be pressed to read the maximum and minimum values of the cutter speed. At the same time, the cutting effect is rated according to the cutting breakage and the morphology of the stalk section, etc. The rating values are from 1 to 10.

3. Results and Discussion

3.1. Analysis of Mechanical Properties of Broccoli Xylem

Figure 9 shows the shear force curve of the first stalk sample; from measurement points 1–5, the maximum shear force shows an increasing trend, and the maximum shear force range is 25.47–41.79 N. The curve is divided into a continuous loading phase and a stable shear phase, and the shear blade displacement ranges corresponding to the continuous loading phase is 4–6 mm; this is consistent with the thickness range of the epidermis and xylem, thus indicating that the shear resistance mainly originates from epidermis and xylem. In the steady shear stage, there was no larger change in shear force, indicating that the pith of the broccoli stalk had less influence on the shear force. The small fluctuations in the shear force curve during the continuous loading and steady shear stages were attributed to the uneven circumferential distribution of the stalk components.

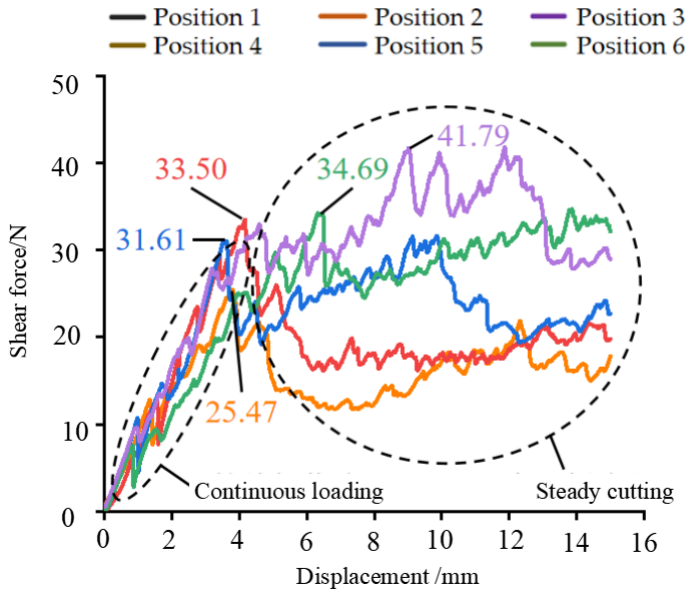

Figure 9. Shear force-displacement characteristic curve of a broccoli stem sample.

Broccoli stalk shear tests showed that shear force fluctuations occur during cutting with a toothless blade and that the thickness of the xylem has a greater effect on the cutting force. This is due to the presence of strips of wood fibers in the broccoli stalk and xylem layer, and the process of cutting off unevenly distributed wood fibers can lead to shear force fluctuations, which can also affect the smooth operation of the cutting unit.

3.2. Simulation Analysis of the Cutting Mechanism of the Xylem Stem

3.2.1. Single Factor Simulation Analysis

In the single-factor simulation of broccoli stalk cutting, to study the effect of a single factor on the cutting effect, the values of the remaining factors were kept at an intermediate level when changing the value of a single factor. The relevant parameters were set according to the table for the solution, and the results of the data obtained from the solution were exported and processed to obtain the simulation results of cutting broccoli stalks with a geared disc cutter, as shown in Figure 10.

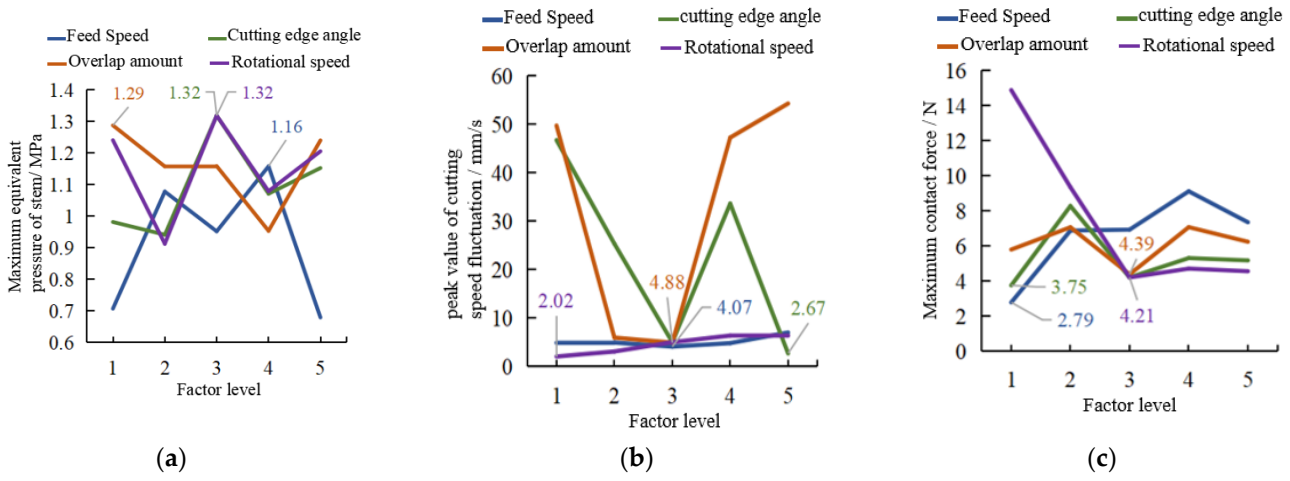

Figure 10. Simulation results of gear disc cutting broccoli stem. (**a**) Maximum equivalent pressure in the stem. (**b**) Peak value of cutter feed rate fluctuation. (**c**) Maximum contact force between cutter and stem.

The maximum equivalent force on the stalk during cutting, when the feed speed of the circular knife is 0.11 m/s and 0.31 m/s, the equivalent force on the broccoli stalk exceeds 1 MPa, which is significantly greater than that when the feed speed is 0.01 and 0.41 m/s, as shown in Figure 10a. When the feed speed is 0.31 m/s, the maximum equivalent force on the broccoli stalk is 1.1579 MPa. The maximum equivalent force on broccoli stalks was 1.3185 MPa at a cutting edge angle of 25 degrees and a cutter speed of 600 rpm. The maximum equivalent force on stalks was 1.2874 MPa at a cutter disc overlap of 1 mm. A greater equivalent force on stalks indicates a greater cutting force provided by the cutter. To maximize the stalk equivalent force, the optimal cutter operating parameters were: 0.31 m/s feed rate, 25-degree cutting edge angle, 1 mm overlap, and 600 rpm.

During the cutting process, the cutter will be subjected to resistance, and the unbalanced impact leads to unstable cutter operation. In addition, the cutter's advance speed will vary with the ups and downs around the set value, which will be defined as the cutter's advance speed fluctuation. As shown in Figure 10b, the feed speed and speed variation have less of an effect on the cutting tool advance speed fluctuation. The peak value of the cutting tool advance speed fluctuation varies more when different values of the cutting edge angle and the overlap are taken. To ensure the cutter runs smoothly and the peak of forward speed fluctuation is less than 5 mm/s, a cutting edge angle of 25 or 45 degrees and a blade overlap of 11 mm are more suitable.

The maximum contact force tends to increase as the feed speed increases, which means that a larger feed speed will cause a greater impact force, as shown in Figure 10c. The contact force is at a maximum when the cutting edge angle is 15 degrees, and the contact force is about 4 N when the rest of the factors are chosen to be horizontal. The contact force is minimum when the blade overlap is 11 mm. The contact force decreases with the increase in cutter speed, and the smaller the cutter speed, the larger the contact force, which indicates that the impact force on the cutter is larger when cutting. The contact force between the cutter and the stalk will cause stress concentration on the cutter and damage to the structure of the cutter and also affect the smooth operation of the cutter. Therefore, a feed speed of 0.01 m/s, a cutting edge angle of 5 degrees, a blade overlap of 11 mm, and a cutter speed of 600 rpm are the best operating parameters.

Broccoli stalk cutting is a process of interaction between the disc cutter and the stalk, and the cutting effect is related to the stress state of the stalk and the running state of the cutter. Combining the single-factor simulation results with the actual situation analysis, the operating parameters of the geared Cutter I are a 0.21–0.31 m/s feed speed, 5–25 degrees cutting edge angle, 1–11 mm overlap between the two cutters, and 600~1000 rpm cutter speed to produce a larger equivalent force and larger shear force on the broccoli stalk, and at the same time to ensure the smooth operation and cutting efficiency of the disc cutter.

3.2.2. Multi-Factor Simulation Analysis

The four-factor, three-level orthogonal test simulations using the Box–Behnken design in Design-Expert 10 software are shown in Table 3. A total of 29 simulations were conducted and the maximum equivalent force of the geared disc cutter cutting the stalk, the peak of the cutter forward speed fluctuation, and the maximum contact force of the cutter stalk during the simulation were counted.

The maximum stalk equivalent force Y_1 for Group 28 simulation is the largest at 1.2632 MPa, and the combination of factors at this time comprises a feed speed of 0.31 m/s, cutting edge angle of 15 degrees, cutter overlap of 1 mm, and cutter speed of 800 rpm, as shown in Table 3. The maximum contact force Y_3 of the cutter stalk in the 25th group was the smallest at 4.5008 N. The combination of factors comprised 0.26 m/s of feed speed, 5 degrees of cutting edge angle, 6 mm of cutter overlap, and 1000 rpm of cutter speed.

Table 3. Orthogonal simulation experiment of gear disc cutter cutting a broccoli stem.

Run	Factor				Response		
	A/m/s	B/Degrees	C/mm	D/rpm	Y_1/MPa	Y_2/mm/s	Y_3/N
1	0.26	15	6	800	1.1449	37.28	6.9046
2	0.31	25	6	800	1.205	9.31	6.4028
3	0.21	15	11	800	1.1303	22.47	7.3324
4	0.26	25	6	1000	0.91934	10.86	7.4814
5	0.26	15	1	1000	1.2541	40.86	5.7459
6	0.21	15	6	1000	0.99954	35.96	5.4476
7	0.21	5	6	800	1.1675	62.7	8.5025
8	0.21	15	6	600	1.254	28.27	7.2396
9	0.26	5	1	800	1.1789	28.92	7.0209
10	0.26	25	6	600	1.2312	6.39	5.5769
11	0.21	15	1	800	1.1304	33.58	6.8834
12	0.26	15	6	800	1.2498	38.66	7.8081
13	0.26	15	11	1000	1.1674	23.33	5.7599
14	0.26	25	11	800	0.8733	27.07	4.5833
15	0.26	5	6	600	1.08	49.16	9.7256
16	0.21	25	6	800	1.1414	7.96	5.8652
17	0.26	15	6	800	1.1449	37.28	6.9046
18	0.31	15	6	600	0.95669	29.37	12.6
19	0.26	15	1	600	1.1348	24.7	9.184
20	0.26	15	6	800	1.1449	37.28	6.9046
21	0.31	5	6	800	0.99839	62.8	9.6223
22	0.26	15	6	800	1.2498	38.66	7.8081
23	0.31	15	6	1000	1.083	36.4	6.8667
24	0.26	15	11	600	1.2397	17.47	8.3645
25	0.26	25	1	800	1.2388	72.98	4.5008
26	0.26	5	6	1000	0.97838	68.42	8.346
27	0.26	5	11	800	1.0158	73.05	6.3209
28	0.31	15	1	800	1.2632	33.29	9.1501
29	0.31	15	11	800	0.85783	23.03	6.6314

The mathematical equations obtained by fitting the experimental data may produce inaccurate results; thus, it is necessary to use an analysis of variance (ANOVA) to test the significance and accuracy of the models [27]. ANOVA was performed for the three response models of the simulation results, and the fitting statistics of the three models are shown in Table 4. The ratio of the standard deviation to the mean is called the coefficient of variation, and the coefficient of variation for all three models was less than 20%. The goodness of fit was 0.9207, 0.9995, 0.8906, and 0.9798, which indicates that the regression equations are in good agreement with the simulation results and that the established models can reflect the simulation data well. The signal-to-noise ratios (Adeq Precision) of the three models were 6.8398, 138.4123, and 22.8585, respectively. In the Design-Expert software, a signal-to-noise ratio greater than 4 is desirable, so the three models fitted are reliable.

Table 4. Fitting effect of the models.

Model	Standard Deviation	Average Value	Coefficient of Variation/%	Coefficient of Determination	Signal-to-Noise Ratio
Stem maximum equivalent stress (Y_1)	0.068	1.12	6.08	0.9207	6.8398
Advance speed fluctuation peak value (Y_2)	0.626	35.09	1.79	0.9995	138.4123
Maximum contact force (Y_3)	0.429	7.29	5.88	0.9798	22.8585

Figure 11 shows the distribution of the residuals outside the studentification fitted by the three models. Figure 11a shows the residuals fitted by the stalk maximum equivalent

force model: the maximum residual value is 2.773, and the rest of the residual values are within ±2. Figure 11b shows the residuals fitted by the model of peak cutter forward velocity fluctuation: the residuals are all within ±2, and the maximum residual is 1.861. Figure 11c shows the residuals fitted by the model of maximum contact force: the residuals are all within ±2, and the maximum residual is 1.51. According to the student's external residual plot, the three models are well fitted, and the residuals are all within a small range.

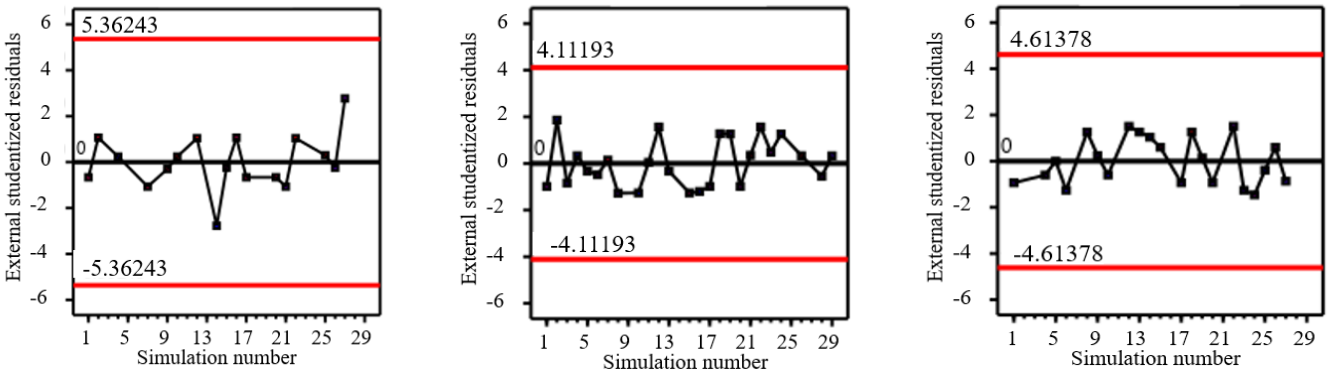

(**a**) (**b**) (**c**)

Figure 11. Externally studentized residuals of the model. (**a**) Maximum equivalent stress of stem. (**b**) Peak value of the cutter blade feed rate fluctuation model. (**c**) Maximum contact force.

Figure 12 shows the comparison of model prediction and simulation results. The horizontal coordinates of the points in the figure indicate the simulation results, and the vertical coordinates indicate the values predicted by the model. The closer the horizontal and vertical coordinates of the data points are, the closer the true value of the point is to the predicted value and the smaller the error. Figure 12a shows the comparison between the model-predicted value of the maximum equivalent force of the stalk and the simulation results. The simulation results of the maximum equivalent force of the stalk range from 0.85783 to 1.2632 MPa and the points are evenly distributed on both sides of the line. Figure 12b shows the comparison between the model prediction and simulation results of the peak fluctuation of the cutting knife forward speed. The simulation results of the peak fluctuation of the cutting knife forward speed are 6.39 mm/s at the minimum and 73.05 mm/s at the maximum, and all points are on a straight line, which indicates that the model fits well and the values solved according to the model are very close to the simulation results. Figure 12c shows the comparison between the predicted values of the maximum contact force model and the simulation results. The simulated maximum contact force is 4.5008–12.6 MPa, and the data points are uniformly distributed on both sides of the straight line.

To obtain the optimal operating parameters for the geared disc cutter cutting broccoli stalks, the Optimization function in Design-Expert software was used to provide the solution; the constraints and response objectives of the solution process are shown in Table 5. The solution objectives of the factors are all within the upper and lower limits, and the stalk equivalent force represents the cutting force, so the solution objective is to maximize the maximum stalk equivalent force. The peak cutter forward speed fluctuation and the maximum contact force have an impact on the smoothness of cutter operation, so the solution objective is to converge to zero.

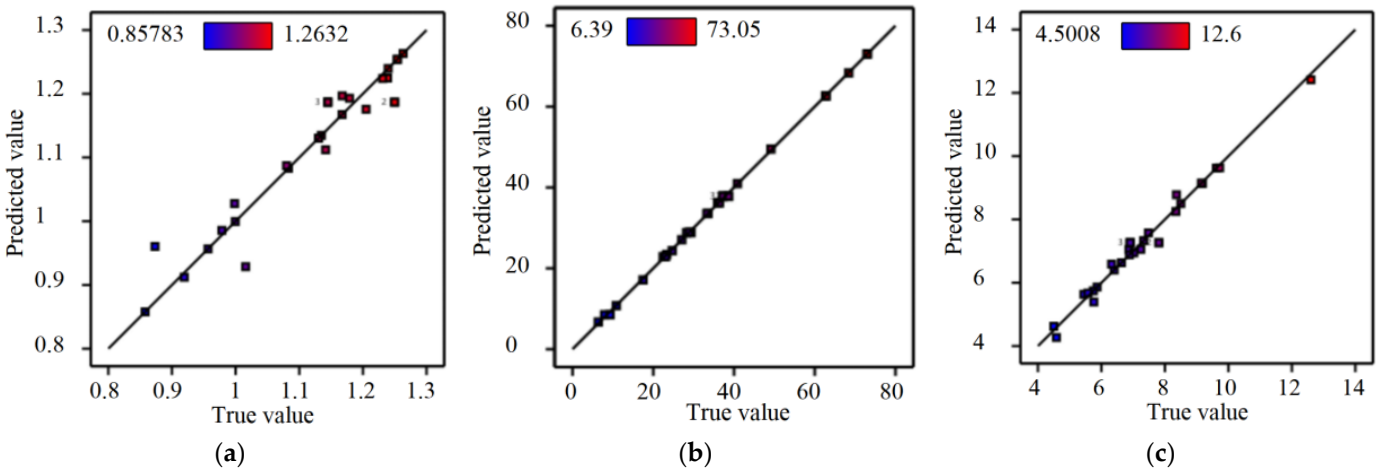

Figure 12. Comparison plot between predicted values of the model and simulation results. (**a**) Maximum equivalent stress of stem. (**b**) Peak value of the cutter blade feed rate fluctuation. (**c**) Maximum contact force.

Table 5. Constraints for solving optimization.

	Name	Units	Lower Limit	Upper Limit	Solution Objective	Upper Weight	Lower Weight	Significance
Factor	A: Feed rate	m/s	0.21	0.31	Within range	1	1	3
	B: Cutting edge angle	degree	10	35	Within range	1	1	3
	C: Overlap amount	mm	1	11	Within range	1	1	3
	D: Rotational speed	rpm	400	1000	Within range	1	1	3
Response	Y_1: Stem maximum equivalent stress	MPa	0	1.5	maximize	1	1	3
	Y_2: Advance speed fluctuation peak value	mm/s	0	5	It goes to 0	1	1	3
	Y_3: Maximum contact force	N	0	10	It goes to 0	1	1	3

The optimal parameters and response obtained from the solution are shown in Figure 13, and the desirability of the solution result is a value of one. The optimal operating parameters of the cutting device are a forward speed of 0.239 m/s, a cutting edge angle of 30.974 degrees, a cutter overlap of 10.066 mm, and a rotational speed of 467.511 rpm. Under the optimal working parameters, the maximum stem equivalent stress is 1.786 MPa, the maximum peak value of cutting feed fluctuation is zero, and the maximum contact force is zero.

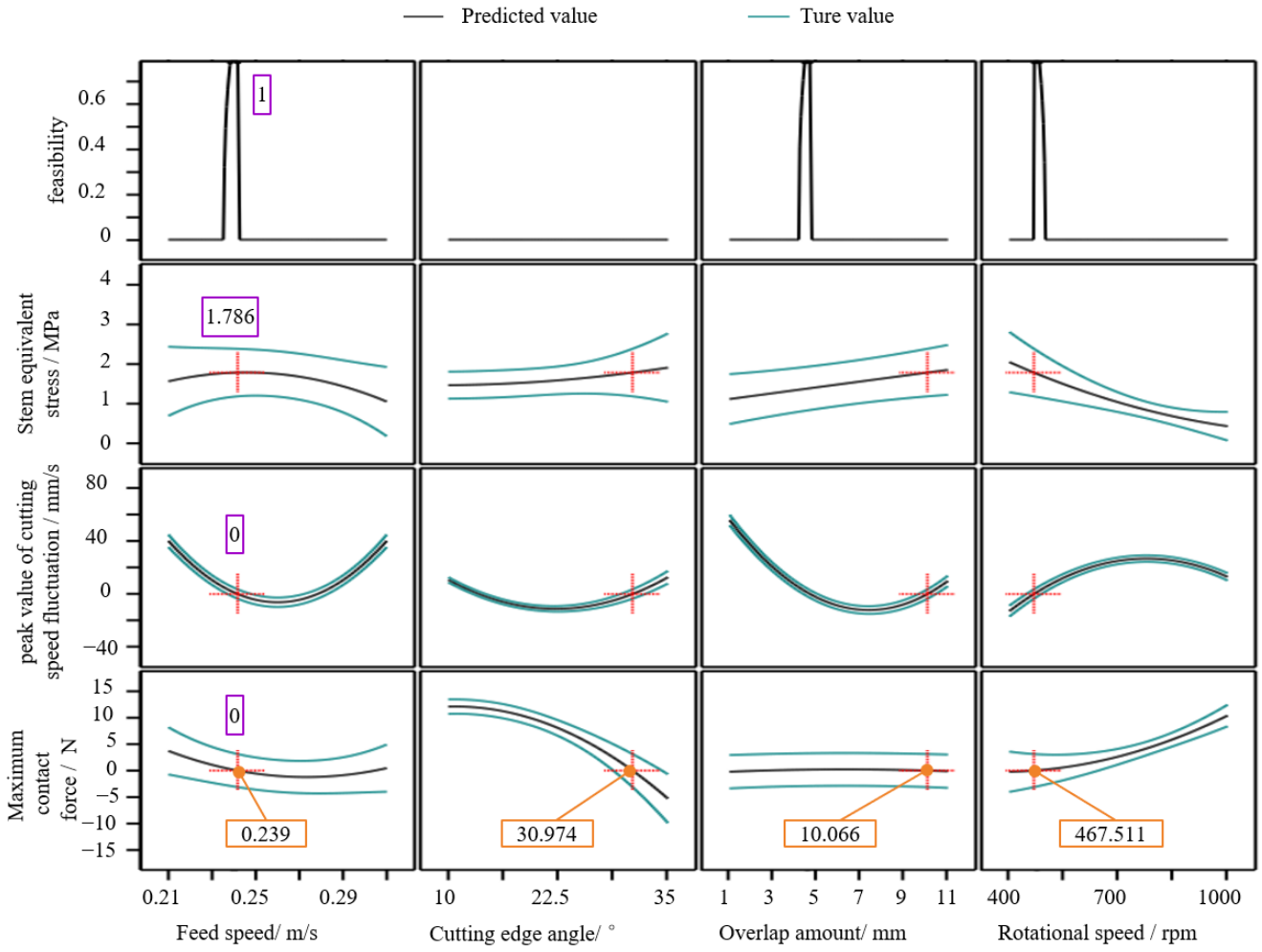

Figure 13. Optimization results for the factors and responses.

3.3. Analysis of the Bionic Cutter Blade Cutting Teeth Profile Curve

The curve fitting was debugged and analyzed using Origin software with fitting and plotting functions. The obtained two-dimensional coordinate data of the pixel points of the three curves were imported into Origin software and fitted using the Polynomial Fit command. Since the waveform curve characteristics are more suitable for the polynomial fitting method, to ensure the fitting accuracy, the curve fitting results were made to coincide with the locust tangent lobe boundary contour curve by continuously conducting the equation order. The final fitting method was determined as a least-squares eight polynomial, and the fitting equation is:

$$\varphi(x) = intercept + B_1x + B_2x^2 + B_3x^3 + B_4x^4 + B_5x^5 + B_6x^6 + B_7x^7 + B_8x^8 \quad (1)$$

The results of fitting the equation parameters are shown in Table 6. The coefficients of determination R_2 are all greater than 0.987, and the accuracy of the fitted equations is high.

Table 6. Results of curve fitting.

	Curve 1		Curve 2		Curve 3	
	Result	**Standard Error**	**Result**	**Standard Error**	**Result**	**Standard Error**
Intercept	104.77	1.2600	110.83	0.55521	114.58	1.5087
B_1	4.1579	0.69271	2.8605	0.31264	9.6237	0.90430
B_2	−0.94490	0.12506	−0.30522	0.057840	−1.1505	0.17834
B_3	0.095042	0.010438	0.016811	0.0049495	0.067894	0.016290
B_4	−0.0044191	4.6658×10^{-4}	-3.3242×10^{-4}	2.2690×10^{-4}	−0.0020354	7.9777×10^{-4}
B_5	1.0906×10^{-4}	1.1869×10^{-5}	-1.0201×10^{-6}	5.9204×10^{-6}	3.0457×10^{-5}	2.2247×10^{-5}
B_6	-1.4862×10^{-6}	1.7200×10^{-7}	1.2500×10^{-7}	8.8017×10^{-8}	-1.7666×10^{-7}	3.5359×10^{-7}
B_7	1.0587×10^{-8}	1.3214×10^{-9}	-1.6221×10^{-9}	6.9372×10^{-10}	-4.4679×10^{-10}	2.9800×10^{-9}
B_8	-3.0831×10^{-11}	4.1737×10^{-12}	6.7599×10^{-12}	2.2481×10^{-12}	6.6607×10^{-12}	1.0328×10^{-11}
R_2	0.99411		0.99854		0.98729	

Curve 1 fitted by Origin software is shown in Figure 14a, with 78-pixel points. The curve shows a rising and then decreasing trend, with a peak value of 144.347. The distribution of the fitted residuals is shown in Figure 14b, and the residuals are all distributed within ±3, which is a good fit. The equation of Curve 1 is:

$$\varphi(x) = 104.77 + 4.1579x - 0.9449x^2 + 0.095042x^3 - 0.0044191x^4 + 1.0906 \times 10^{-4}x^5 - 1.4862 \times 10^{-6}x^6 + 1.0587 \times 10^{-8}x^7 - 3.0831 \times 10^{-11}x^8 \quad (2)$$

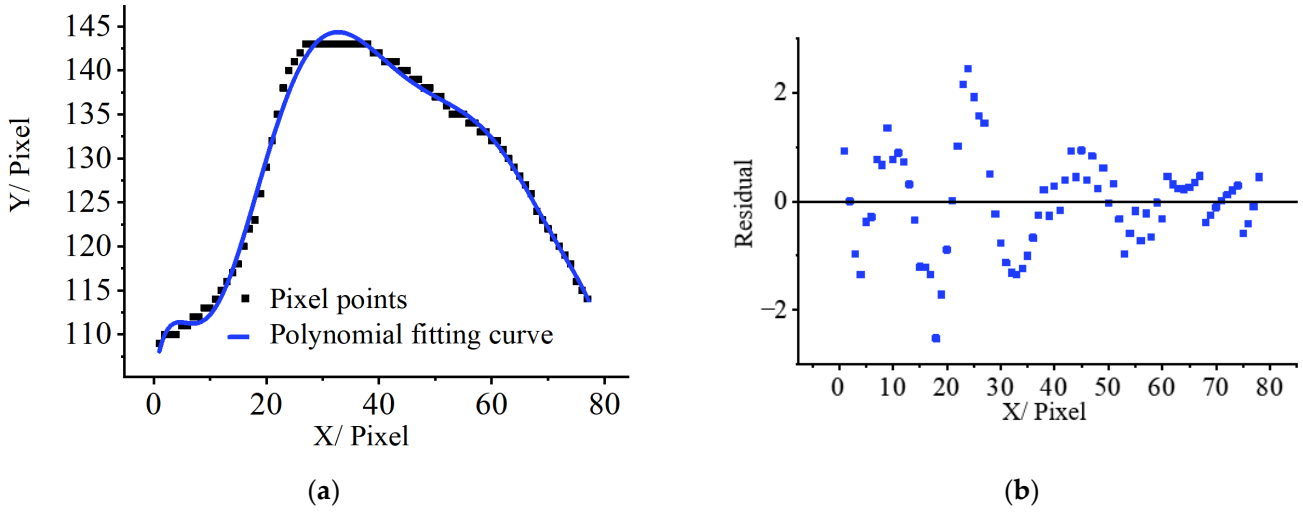

Figure 14. Fitting results of Curve 1. (**a**) Tooth profile of Curve 1. (**b**) Residual distribution plot.

The curve fitted by Origin software is shown in Figure 15a. There are 76-pixel points, the curve shows a rising trend and then a falling trend, and the peak of the curve is 147.986. The distribution of the fitted residuals is shown in Figure 15b; the residuals are all distributed in the range of ±2, and the fitting effect is good. The equation of Curve 2 is:

$$\varphi(x) = 110.83 + 2.8605x - 0.30522x^2 + 0.016811x^3 - 3.3242 \times 10^{-4}x^4 - 1.0201 \times 10^{-6}x^5 + 1.25 \times 10^{-7}x^6 - 1.6221 \times 10^{-9}x^7 + 6.7599 \times 10^{-12}x^8 \quad (3)$$

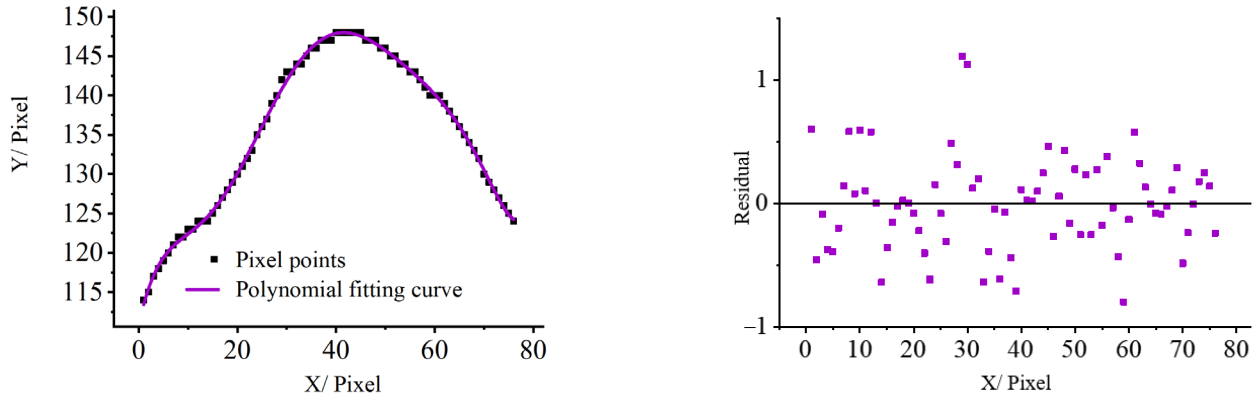

(**a**) (**b**)

Figure 15. Fitting results of Curve 2. (**a**) Tooth profile of Curve 2. (**b**) Residual distribution plot.

Curve 3 fitted by Origin software is shown in Figure 16a. There are 71-pixel points, the curve shows a rising trend and then a decreasing trend, and the peak of the curve is 159.714. The distribution of the fitted residuals is shown in Figure 16b; the residuals are all distributed in the range of ±3, and the fitting effect is good. The equation of Curve 3 is:

$$\varphi(x) = 114.58 + 9.6237x - 1.1505x^2 + 0.067894x^3 - 0.0020354x^4 + 3.0457 \times 10^{-5}x^5 \\ -1.7666 \times 10^{-7}x^6 - 4.4679 \times 10^{-10}x^7 + 6.6607 \times 10^{-12}x^8 \quad (4)$$

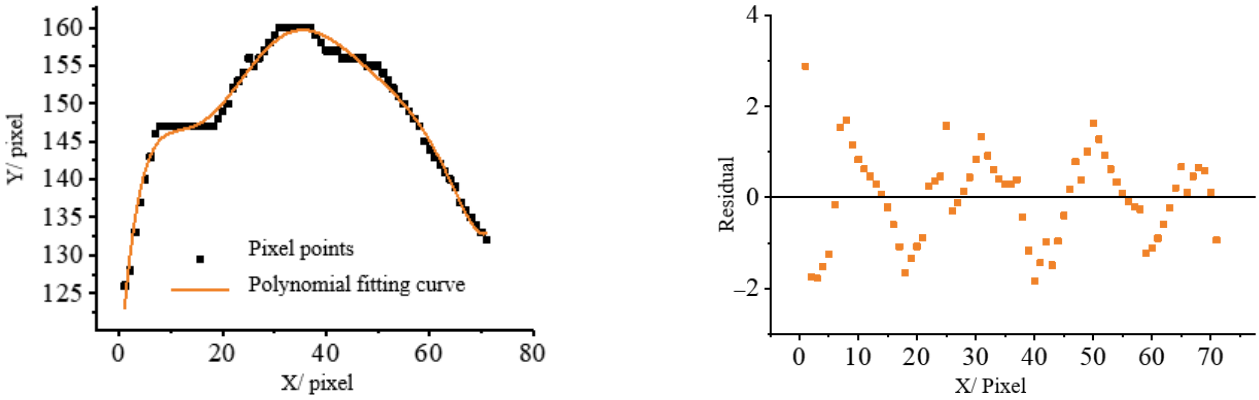

(**a**) (**b**)

Figure 16. Fitting results of Curve 3. (**a**) Tooth profile of Curve 3. (**b**) Residual distribution plot.

3.4. Design and Testing of Biomimetic Cutter

According to the structure and parameters of the disc cutter designed above, the diameter of the disc cutter is 220 mm, the thickness is 2 mm, the number of teeth is 48, and the cutting edge angle is 16 degrees. In Solid Works software, the equations of the three curves were used to draw the disc cutter edge curves, respectively. The 3D model of the disc cutter established with Curve 2 as an example is shown in Figure 17. The model should be saved as a file with the suffix ".x_t".

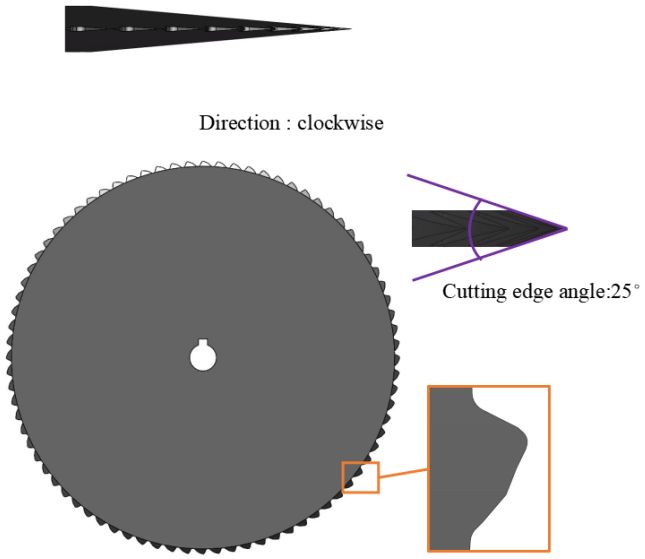

Figure 17. Bionic disc cutter 3D model.

The impact load generated by the collision between the high-speed rotating tool and the stalk will cause a strong vibration of the tool and lead to deformation of the tool. The vibration of the tool mainly has three directions: axial vibration, radial vibration, and torsional oscillation. When the vibration frequency of the tool is close to its inherent frequency, the tool will resonate and this leads to large deformation, which will damage the tool. To avoid the large deformation of the tool due to resonance and thus affecting the cutting effect, it is necessary to conduct a modal analysis of the tool to ascertain its inherent frequency before conducting other dynamic simulation analyses.

The model file of the disc cutter is imported into ANSYS FEA software for modal analysis. The material of the disc cutter is tool steel with a density of 7850 kg/m^3, modulus of elasticity of 2 × 1011 Pa, and Poisson's ratio of 0.3. As shown in Figure 18, the mesh of the disc cutter is divided into 67,341 nodes and 33,874 solid cells. The disc cutter is affected by centrifugal force when it rotates, so it needs to be solved for pre-stress before the modal analysis solution. The through-hole and keyway in the middle of the disc cutter are used for fixed installation with the shaft, so fixed support is added at the circular hole and the speed of the disc cutter is set to 480 rpm.

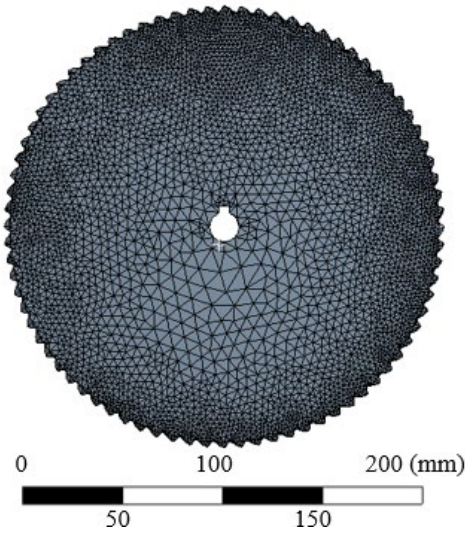

Figure 18. Meshing of bionic disc cutter.

The deformation of the disc cutter obtained by the solver is shown in Figure 19. The deformation of the disc cutter increases gradually from the center of the cutter to the edge, and the maximum deformation is 2.1703 $\times$ 10^{-5} mm, which is located at the edge of the disc cutter. The equivalent force of the disc cutter is shown in Figure 20. The equivalent force decreases gradually from the center of the cutter to the edge, and the maximum equivalent force is 0.16175 MPa, which is located at the keyway of the cutter.

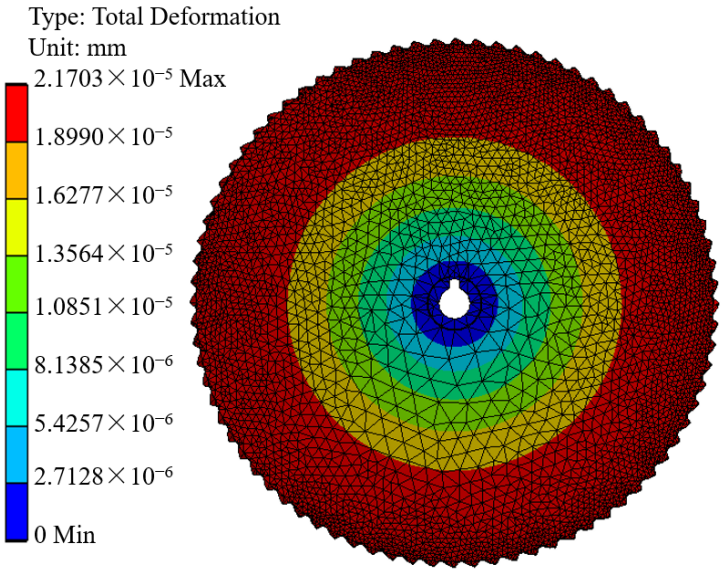

Figure 19. Total deformation of bionic disc cutter.

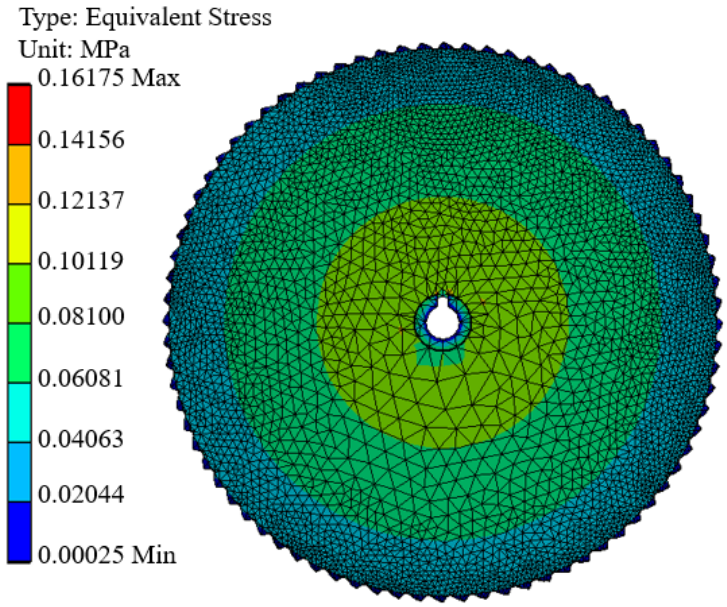

Figure 20. Equivalent stress of bionic disc cutter.

The vibration pattern of the first six steps of the disc cutter is shown in Figure 21. The inherent frequency of the first-order vibration pattern of the disc cutter is 154.72 Hz, and the disc cutter as a whole flips left and right; the inherent frequency of the second-order vibration pattern is 154.84 Hz, and the disc as a whole flips up and down; the inherent frequency of the third-order vibration pattern is 182.28 Hz, and the disc cutter undergoes concave and convex deformation vibration, and the vibration is the largest at the position near the edge; the intrinsic frequencies of the fourth- and fifth-order vibration patterns are

238.3 Hz and 238.26 Hz, respectively, and the disc blade produces a twisted deformation vibration; the intrinsic frequency of the sixth-order vibration pattern is 516.08 Hz, which is a more serious twisted deformation vibration of the disc blade.

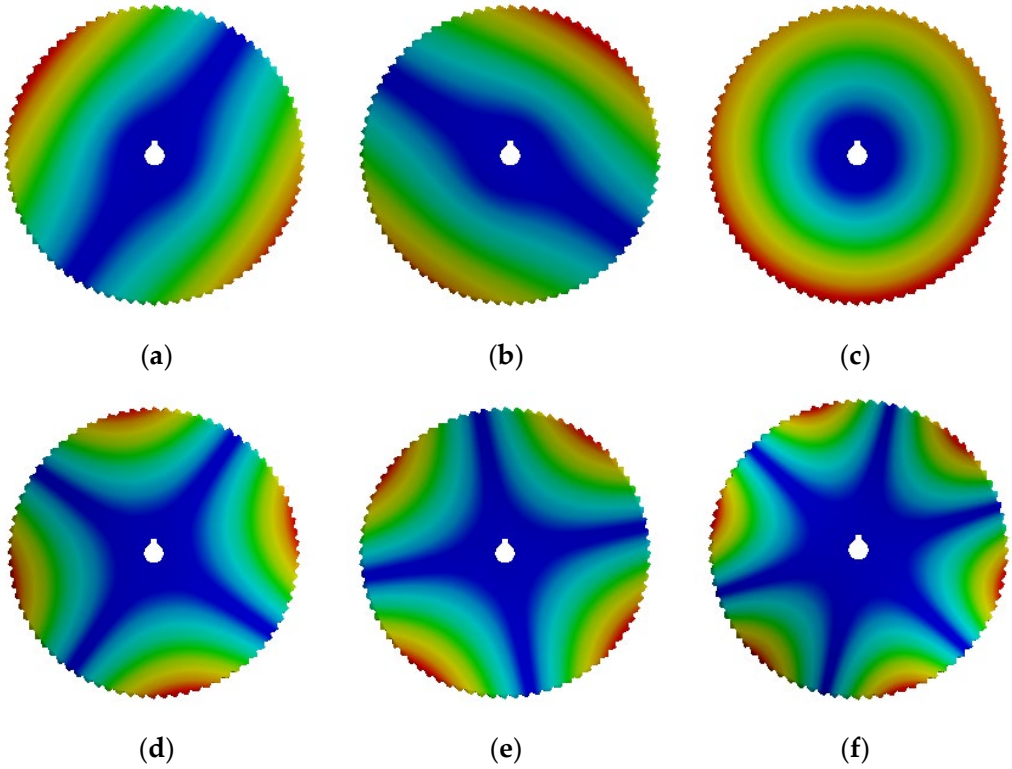

Figure 21. The first six order mode shapes of the pre-stressed bionic circular cutter. (**a**) First order. (**b**) Second order. (**c**) Third order. (**d**) Fourth order. (**e**) Fifth order. (**f**) Sixth order.

The rotational speed parameter of the disc blade set in this paper is 480 rpm, and its corresponding rotational frequency is 8 Hz. Compared with the inherent frequency of the first six orders of vibration patterns obtained above, the rotational speed setting avoids the resonance zone, such that the parameters of the rotational speed and structure of the disc blade are reasonable.

3.5. Biomimetic Cutter Cutting Simulation Analysis

Based on the parameters of the disc cutter determined above and the three tangential leaf curve models established by the bionic, three bionic cutters were created along with one conventional cutter, and their cutting process was simulated and analyzed.

The stalk equivalent force is shown in Figure 22. The maximum equivalent force of stalks cut by different cutters displayed a similar trend. The maximum equivalent force of the conventional cutter cutting the stalk peaked at 1.1458 MPa, which was larger than the maximum equivalent force of the bionic cutter cutting the stalk, which means that the conventional cutter produced a larger cutting force than the bionic cutter at this moment. However, during the cutting process, the maximum stalk equivalent force cut by the bionic cutter was greater than that of the conventional cutter in all cases, and the maximum stalk equivalent force cut by the conventional cutter fluctuated considerably. Therefore, the bionic cutter can provide a larger and more stable cutting force than the conventional cutter.

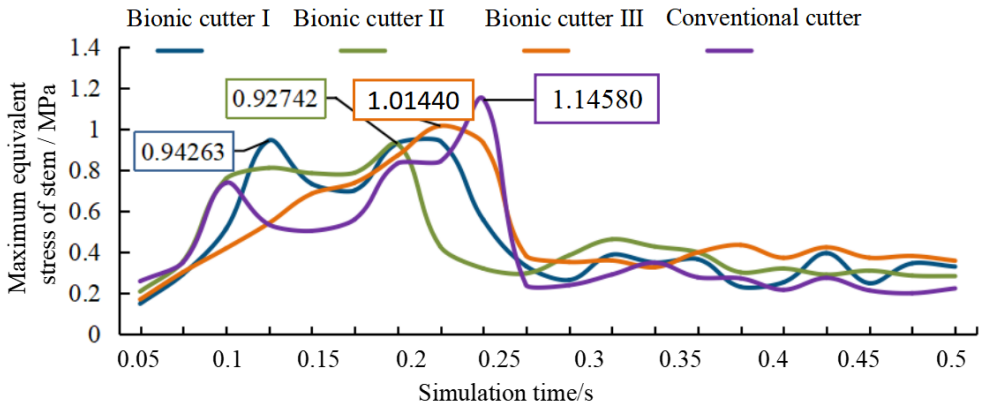

Figure 22. Maximum equivalent stress of the stem during the simulated cutting process.

The peak fluctuation curve of the advancing speed of the cutter in the cutting simulation process is shown in Figure 23. The peak fluctuation of the advancing speed of the conventional cutter was significantly larger than that of the bionic cutter, and the peak fluctuation of each moment had a large fluctuation, which means that the conventional cutter ran less smoothly when it was subject to cutting resistance. The maximum peak fluctuation of the forward speed of the conventional cutter was 42.57 mm/s, which means that at this moment, the forward speed of the simulated cutter differed from the preset forward speed by 42.57 mm/s, which is a large deviation. The peak of forward speed fluctuation of Bionic Cutters I, II, and III were 16.3, 9.17, and 21.93 mm/s, respectively. Bionic Cutter II had a lower fluctuation of forward speed when subjected to cutting resistance and ran more smoothly; thus, it was more suitable for broccoli stalk cutting.

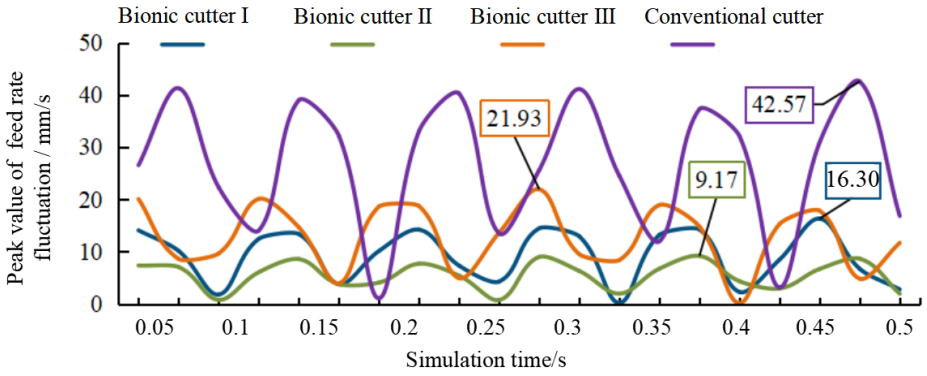

Figure 23. Fluctuation peak of cutter forward speed during the simulated cutting process.

The maximum contact force curve of the cutter stalk during the cutting simulation is shown in Figure 24. The maximum contact force of each cutter displayed the same trend, and the peak points were all located between 0.05 and 0.1 s when the cutter teeth completely cut into the stalk. The maximum contact force between Bionic Cutter I and the stalk was 11.182 N, which was greater than the other cutters, indicating that the impact force on Bionic Cutter I was greater. The contact force between Bionic Cutters II and III and the stalk was smaller than that of the conventional cutter, which indicates that the impact force on the Bionic Cutters II and III was smaller, which is more favorable for the smooth operation of the cutting device and can also reduce the wear of the cutter.

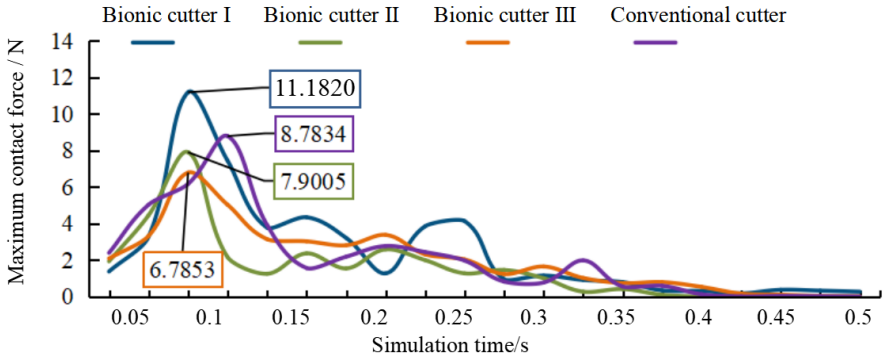

Figure 24. Maximum contact force during the simulated cutting process.

The results of the comparative analysis of the maximum equivalent force of the stalk, the fluctuation of the forward speed of the cutter, and the maximum contact force during the simulation showed that Bionic Cutter II cut the broccoli stalk with more favorable values; thus, Bionic Cutter II was chosen as the broccoli stalk cutter.

3.6. Comparative Experimental Analysis of Test Benches

The test conditions and results for broccoli stalk-cutting designed using Design-Expert software are shown in Table 7. Seventeen trials were conducted for each cutter using a three-factor, three-level orthogonal test method, for a total of 68 trials. The cutter speed fluctuation values were tested at 300, 450, and 600 rpm, a cutter overlap of 0, 7.5, and 15 mm, and a stalk pushing feed speed of 0.1, 0.2, and 0.3 m/s, respectively, while the scoring values of stalk-cutting effectiveness were obtained. Maximum speed fluctuation values of 23.6, 16.1, 16.4, and 17.6 rpm were obtained for Bionic Cutters I–III and a conventional cutter for cutting broccoli stalks, respectively, and the minimum values of the cutting effect were 1, 1, 2, and 1. The combination of operating parameters corresponding to larger speed fluctuation values and smaller scoring values of the cutting effect did not apply to the broccoli stalk-cutting device.

Table 7. Test results of cutting broccoli stem.

Serial Number	X1: Rotational Speed/rpm	X2: Overlap Amount/mm	X3: Putter Speed/m/s	Y: Fluctuation Value of Cutter Rotational Speed/rpm				Z: Cutting Quality Rating			
				Bionic Cutter I	Bionic Cutter II	Bionic Cutter III	Conventional Cutter	Bionic Cutter I	Bionic Cutter II	Bionic Cutter III	Conventional Cutter
1	300	7.5	0.1	14.2	9.3	8.5	17.7	6	4	7	6
2	600	0	0.2	11.2	14.9	12.2	13.7	3	2	5	6
3	450	0	0.3	11.6	10.2	4.7	12.2	1	1	6	1
4	600	7.5	0.1	10.5	8.9	16.2	11.6	5	7	9	7
5	450	7.5	0.2	10.1	6.5	4.6	2.8	8	6	6	8
6	300	0	0.2	11.3	16.1	11.5	14	1	4	2	1
7	600	15	0.2	23.6	5	16.4	11.4	6	6	8	10
8	450	7.5	0.2	8.8	6.3	1.9	7.9	8	8	8	8
9	600	7.5	0.3	8.4	7.4	8.8	9.6	5	5	9	7
10	450	7.5	0.2	3.9	2.5	1.5	0.3	7	5	7	6
11	300	15	0.2	10.8	9.4	9.3	8.1	6	9	8	7
12	450	7.5	0.2	4.9	0.5	4.3	6.1	9	7	9	7
13	300	7.5	0.3	5.3	14.4	10.9	11.3	7	6	6	8
14	450	7.5	0.2	7.1	8.1	6.7	6.2	7	7	8	8
15	450	15	0.3	14.4	7.5	8	5.6	4	8	9	7
16	450	0	0.1	10.9	11.2	11.5	15.7	3	1	3	1
17	450	15	0.1	16.9	4.7	15.9	14.8	7	8	8	7

The quadratic polynomial model fitting and ANOVA were performed in Design-Expert software for the cutter speed fluctuation values and cutting effects. The models established were significant and the misfit term was not significant, and the models established for the true values of each factor were as detailed below.

The model for the rotation speed fluctuation values of Bionic Cutter I is as follows:

$$Y_1 = 45.9650 - 0.1024X_1 - 2.2137X_2 - 96.3000X_3 + 0.0029X_1X_2 + 0.1133X_1X_3 - 1.0667X_2X_3 + 0.0001{X_1}^2 + 0.0988{X_2}^2 + 93.2500{X_3}^2 \quad (5)$$

The model for the rotation speed fluctuation values of Bionic Cutter II is as follows:

$$Y_2 = 44.9200 - 0.1469X_1 - 1.0260X_2 + 1.3500X_3 - 0.0007X_1X_2 - 0.1100X_1X_3 + 1.2667X_2X_3 + 0.0002{X_1}^2 + 0.0442{X_2}^2 + 113.5000{X_3}^2 \quad (6)$$

The model for the rotation speed fluctuation values of Bionic Cutter III is as follows:

$$Y_3 = 49.0375 - 0.1593X_1 - 1.4017X_2 - 47.8750X_3 + 0.0014X_1X_2 - 0.1633X_1X_3 - 0.3667X_2X_3 + 0.0002{X_1}^2 + 0.0664{X_2}^2 + 248.7500{X_3}^2 \quad (7)$$

The model for the rotation speed fluctuation values of the conventional cutter is as follows:

$$Y_4 = 74.0775 - 0.1770X_1 - 1.1303X_2 - 208.4250X_3 + 0.0008X_1X_2 + 0.0733X_1X_3 - 1.9000X_2X_3 + 0.0002{X_1}^2 + 0.0592{X_2}^2 + 408.2500{X_3}^2 \quad (8)$$

Using the Optimization function of Design-Expert software, the optimal value of the cutter speed fluctuation is solved by the established model. In the solution condition setting, the range of cutter speed is 300–600 rpm, the range of overlap is 0–15 mm, the feed speed is 0.1–0.3 m/s, and the solution target is the minimum value of cutter speed fluctuation. The solution results are shown in Figure 25. The minimum values of the speed fluctuation of Bionic Cutters I, II, and III, and the conventional cutter were 6.605, 3.4, 4.042, and 4.107 rpm, respectively.

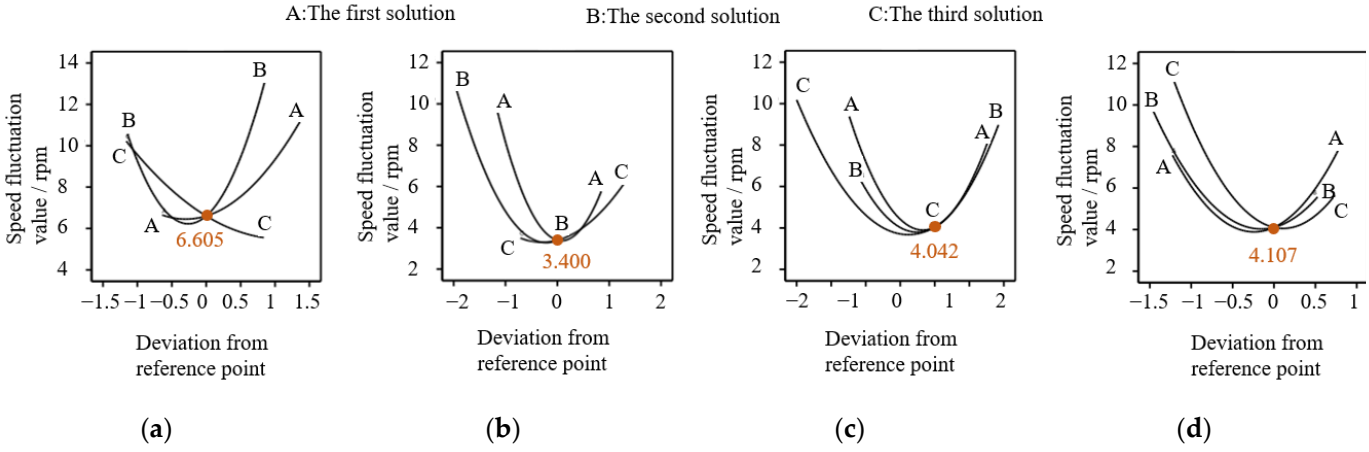

Figure 25. Solution result of minimum fluctuation of the rotational speed of the cutter. (**a**) Bionic Cutter I. (**b**) Bionic Cutter II. (**c**) Bionic Cutter III. (**d**) Conventional cutter.

The model for the effect of the actual values of each factor on the cutting effect of broccoli stems is as detailed below.

The model for the cutting effect score of Bionic Cutter I is as follows:

$$Z_1 = -11.8 + 0.0418X_1 + 1.29X_2 + 51X_3 - 0.0004X_1X_2 - 0.0167X_1X_3 - 0.3333X_2X_3 - 0.00004{X_1}^2 - 0.0516{X_2}^2 - 115{X_3}^2 \quad (9)$$

The model for the cutting effect score of Bionic Cutter II is as follows:

$$Z_2 = -8.35 + 0.0195X_1 + 0.7967X_2 + 67X_3 - 0.0002X_1X_2 - 0.0667X_1X_3 - 0.021{X_2}^2 - 92.5{X_3}^2 \quad (10)$$

The model for the cutting effect score of Bionic Cutter III is as follows:

$$Z_3 = -2.475 + 0.0203X_1 + 1.13X_2 - 16.75X_3 - 0.0007X_1X_2 + 0.0167X_1X_3 - 0.6667X_2X_3 - 0.0276{X_2}^2 + 45{X_3}^2 \quad (11)$$

The model for the cutting effect score of the conventional cutter is as follows:

$$Z_4 = -3.15 - 0.0153X_1 + 1.1533X_2 + 65.5X_3 - 0.0004X_1X_2 - 0.0333X_1X_3 - 0.039{X_2}^2 - 120{X_3}^2 \quad (12)$$

By the same solution method and conditions, the optimal value of the cutting effect is solved by using the above model with the maximum value of the cutting effect as the target, and the results are shown in Figure 26. The optimal values of the cutting effect for Bionic Cutters I, II, III, and the conventional cutter were 7.862, 8.139, 8.811, and 8.374, respectively.

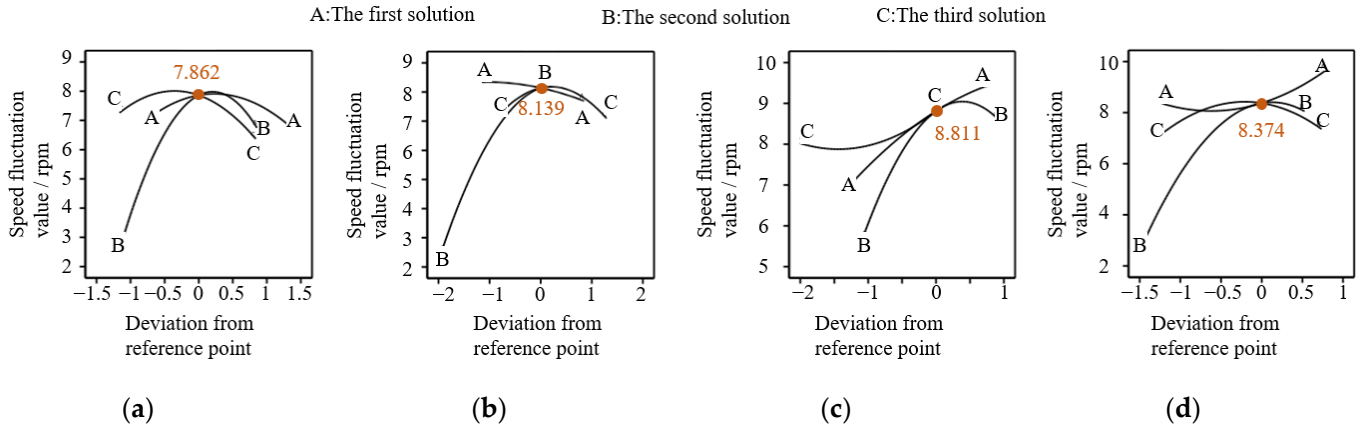

Figure 26. Solution result of optimal cutting effect. (**a**) Bionic Cutter I. (**b**) Bionic Cutter II. (**c**) Bionic Cutter III. (**d**) Conventional cutter.

The operating parameters corresponding to the minimum value of rotational speed fluctuation and the optimum value of the cutting effect for cutting broccoli stalks with the cutter are shown in Table 8. The speed fluctuation value of Bionic Cutter II was the smallest, with only 3.4 rpm at 472.591 rpm, 14.6 mm overlap, and 0.171 m/s feed rate, which means that Bionic Cutter II cut broccoli stalks more smoothly without large speed fluctuations undercutting resistance and impact load. The best cutting effect of Bionic Cutter III was achieved with a cutting effect score of 8.811 at 485.855 rpm, 8.09 mm overlap, and 0.3 m/s feed rate, indicating that the broccoli stalks cut by Bionic Cutter III under this condition had a flat section and no breakage or tear.

Table 8. Optimum operating parameters and cutting effect of cutter.

Cutter	Rotational Speed/rpm	Overlap Amount/mm	Feed Rate/m/s	Minimum Fluctuation of Speed/rpm	Optimal Value of the Cutting Effect	Desirability
Bionic Cutter I	395.905	8.586	0.216	6.606	7.863	0.741
Bionic Cutter II	472.591	14.6	0.171	3.401	8.14	0.791
Bionic Cutter III	485.855	8.09	0.3	4.042	8.811	0.809
Conventional cutter	483.666	11.054	0.226	4.107	8.374	0.793

The minimum value of speed fluctuation that Bionic Cutter I can achieve is greater than the rest of the cutters, and the optimal value of the cutting effect is less than the rest of the cutters; thus, Bionic Cutter I is not suitable for cutting broccoli stalks. To ensure that the cutting effect of the broccoli stalk meets the requirements, it is more appropriate to select the best bionic cutter (Cutter III) as the cutting knife for the broccoli stalk-cutting device.

4. Conclusions

1. Broccoli stalks and xylem contain strips of wood fibers in the xylem layer, which provide a higher degree of tensile and shear resistance than the other components; thus, the cutting of stalks with the xylem often creates problems of constant cutting or unequal cuts. In contrast, in nature, the serrated teeth of many animals have a good cutting effect on cellulose-rich crop stalks. Therefore, inspired by the shaped teeth of locust serrated edges, to optimize the cutting effect of broccoli stalks, this paper designs a bionic disc cutter with serrated edges to cut broccoli stalks.
2. The structure of the cutter edge that imitates the grasshopper-type upper jaw cutting teeth of the East Asian flying locust is an improvement on the original toothless cutter, and based on the contour curve of the locust's upper jaw cutting teeth leaf, a regression equation is established to accurately fit the contour curve of the cutting teeth for designing the bionic cutter. The designed bionic cutter can provide a larger and more stable cutting force than the conventional toothless cutter, as well as a smoother operation of the cutting device and reduced wear and tear on the cutter.
3. The results of the stalk-cutting tests indicated that the speed fluctuation of the conventional toothless disc knife cutting broccoli stalks was greater than that of the bionic knife: the conventional toothless knife repeatedly failed to cut the stalks several times, while the Bionic Cutter III had the best cutting effect and could be effectively used in the actual harvest.

Author Contributions: Conceptualization, Z.T.; methodology, Y.Y. and Z.T.; validation, Y.C., Y.Z. and X.G.; formal analysis, Y.Y.; data curation, Y.Y. and S.L.; investigation, S.C. and Y.Z.; writing—original draft preparation, Y.Y. and Y.C.; writing—review and editing, Y.Z.; supervision, S.C. All authors have read and agreed to the published version of the manuscript.

Funding: This research work was supported by the Single Technology Research and Development Project of Jiangsu Agricultural Science and Technology Innovation Fund (CX (21)3144), the Jiangsu Province and Education Ministry Co-Sponsored Synergistic Innovation Center of Modern Agricultural Equipment (XTCX2007), and the Jiangsu University College Students Practice Innovation Training Program Project (202210299948X).

Data Availability Statement: The data used to support the findings of this study are available from the corresponding author upon request.

Conflicts of Interest: The authors declare no conflict of interest.

References

1. Paśko, P.; Zagrodzki, P.; Okoń, K.; Prochownik, E.; Krośniak, M.; Galanty, A. Broccoli Sprouts and Their Influence on Thyroid Function in Different In Vitro and In Vivo Models. *Plants* **2022**, *11*, 2750. [CrossRef]
2. Li, Z.; Zheng, S.; Liu, Y.; Fang, Z.; Xu, D. Characterization of glucosinolates in 80 broccoli genotypes and different organs using uhplc-triple-tof-ms method. *Food Chem.* **2020**, *334*, 127519. [CrossRef] [PubMed]
3. Loredana, L.; Francesca, M.; Florinda, F.; Filomena, N.; Paola, O.; Donatella, A. Effect of argon-enriched modified atmosphere on the over quality and bioactive compounds of ready-to-use broccoli rabe (*Brassica rapa sylvestris* L. var. esculenta) during the storage. *Food Sci. Technol. Int.* **2023**, *29*, 84–94. [CrossRef]
4. Huang, J.; Liu, Y.; Han, F.; Ji, J. Genetic diversity and population structure analysis of 161 broccoli cultivars based on snp markers. *Hortic. Plant J.* **2021**, *7*, 423–433. [CrossRef]
5. Antonio, C.; Moreno, D.A.; Periago, P.M.; Cristina, G.; Raúl, D. A new food ingredient rich in bioaccessible (poly)phenols (and glucosinolates) obtained from stabilized broccoli stalks. *Foods* **2022**, *11*, 1734.
6. Du, Z.; Sheng, M. Determination of shearing force by measuring NDF and ADF in tea stems with hyperspectral imaging technique. *IFAC Pap.* **2018**, *51*, 849–854.
7. Zhao, Y.F.; Tang, Z.; Chen, S.R. Loading Model and Mechanical Properties of Mature Broccoli (*Brassica oleracea* L. Var. Italica Plenck) Stems at Harvest. *Agriculture* **2022**, *12*, 1519. [CrossRef]
8. Oliveira, M.; Abadias, M.; Vinas, I.; Usall, J.; Torres, R.; Teixido, N. Application of modified atmosphere packaging as a safety approach to fresh-cut fruits and vegetables—A review. *Trends Food Sci. Technol.* **2015**, *46*, 13–26. [CrossRef]
9. Cui, S.Q.; Yu, X.L.; Chen, Y.; Zhang, J.L.; Liu, G.M. Bacterial Diversity and Dominant Spoilage Microorganisms in Fresh-Cut Broccoli. *Appl. Sci.* **2022**, *12*, 3370. [CrossRef]

10. Guan, Y.; Hu, W.; Jiang, A.; Xu, Y.; Yu, J.; Zhao, M.; Ji, Y.; Feng, K.; Sarengaowa; Yang, X. Influence of cut type on quality, antioxidant substances and antioxidant activity of fresh-cut broccoli. *Int. J. Food Sci. Technol.* **2020**, *55*, 3019–3030. [CrossRef]
11. Taghinezhad, J.; Alimardani, R.; Jafary, A. Models of mechanical cutting parameters in terms of moisture content and cross section area of sugarcane stalks. *Agric. Eng. Int. CIGR J.* **2014**, *16*, 280–288.
12. Yinggang, O.; Wegener, M.; Dantong, Y.; Qingting, L.; Dingke, Z.; Meimei, W.; Haochun, L. Mechanization technology: The key to sugarcane production in china. *Int. J. Agric. Biol. Eng.* **2013**, *6*, 1–27.
13. Xu, L.; Yao, H. Research on shear characteristics of chinese cabbage rootstalk. *Agric. Mech. Asia Afr. Lat. Am.* **2009**, *40*, 30–34.
14. Du, D.D.; Wang, J.; Qiu, S.S. Analysis and test of splitting failure in the cutting process of cabbage root. *Int. J. Agric. Biol. Eng.* **2015**, *8*, 27–34.
15. Igathinathane, C.; Womac, A.R.; Sokhansanj, S. Corn stalk orientation effect on mechanical cutting. *Biosyst. Eng.* **2010**, *107*, 97–106. [CrossRef]
16. Tian, K.P.; Li, X.; Zhang, B.; Chen, Q.M.; Shen, C.; Huang, J.C. Design and Test Research on Cutting Blade of Corn Harvester Based on Bionic Principle. *Appl. Bionics Biomech.* **2017**, *2017*, 6953786. [CrossRef]
17. Meyers, M.; Lin, A.; Lin, Y. The cutting edge: Sharp biological materials. *JOM* **2008**, *60*, 19–24. [CrossRef]
18. Wang, J.W.; Guan, R.; Gao, P.X.; Zhou, W.Q.; Tang, H. Design and Experiment of Single Disc to Top Cutting Device for Carrot Combine Harvester. *Nongye Jixie Xuebao/Trans. Chin. Soc. Agric. Mach.* **2020**, *51*, 73–81.
19. Tang, H.; Jiang, Y.; Wang, J.; Guan, R.; Zhou, W. Bionic design and parameter optimization of rotating and fixed stem- and leaf-cutting devices for carrot combine harvesters. *Math. Probl. Eng.* **2021**, *2021*, 8873965. [CrossRef]
20. Guan, C.S.; Fu, J.J.; Xu, L.; Jiang, X.Z.; Wang, S.L.; Cui, Z.C. Study on the reduction of soil adhesion and tillage force of bionic cutter teeth in secondary soil crushing. *Biosyst. Eng.* **2022**, *213*, 133–147. [CrossRef]
21. Zhao, J.; Guo, M.; Lu, Y.; Huang, D.; Zhuang, J. Design of bionic locust mouthparts stubble cutting device. *Int. J. Agric. Biol. Eng.* **2020**, *13*, 20–28. [CrossRef]
22. Wang, M.; Yan, B.; Zhang, S.; Fan, P.; Zeng, P.; Shi, S.; Yang, F. Development of a Novel Biomimetic Mechanical Hand Based on Physical Characteristics of Apples. *Agriculture* **2022**, *12*, 1871. [CrossRef]
23. Du, Z.; Li, D.; Ji, J.; Zhang, L.; Li, X.; Wang, H. Bionic Optimization Design and Experiment of Reciprocating Cutting System on Single-Row Tea Harvester. *Agronomy* **2013**, *12*, 1309. [CrossRef]
24. Du, Z.; Hu, Y.; Lu, Y.; Pang, J.; Li, X. Design of structural parameters of cutters for tea harvest based on biomimetic methodology. *Appl. Bionics Biomech.* **2021**, *2021*, 8798299. [CrossRef] [PubMed]
25. Luo, K.; Wu, Z.M.; Cao, C.M.; Qin, K.; Zhang, X.C.; An, M.H. Biomechanical Characterization of Bionic Mechanical Harvesting of Tea Buds. *Agriculture* **2022**, *12*, 1361. [CrossRef]
26. Wang, Q.; Liu, Y.S.; Yin, X.C. Comparison of Gut Bacterial Communities of *Locusta migratoria* manilensis (Meyen) Reared on Different Food Plants. *Biology* **2022**, *11*, 1347. [CrossRef]
27. Li, C.Y.; Jia, H.L.; Zhang, Z.H.; Wang, G.; Wang, H.C. Grasshopper [chondracris rosea rosea (de geer)] incisors cutting edge contour data extraction and quantitative analysis. *Appl. Mech. Mater.* **2014**, *461*, 144–151. [CrossRef]